J. Wind Eng. Ind. Aerodyn. 99 (2011) 400–413

Contents lists available at ScienceDirect

Journal of Wind Engineering and Industrial Aerodynamics

journal homepage: www.elsevier.com/locate/jweia

Validation of the computational fluid–structure interaction simulation at real-scale tests of a flexible 29 m umbrella in natural wind flow

A. Michalski [a,*], P.D. Kermel [b], E. Haug [b], R. Löhner [c], R. Wüchner [d], K.-U. Bletzinger [d]

[a] Architectural Office Rasch+Bradatsch, Stuttgart, Germany
[b] ESI France, France
[c] George Mason University, Fairfax, Virginia, USA
[d] Chair of Structural Analysis, Technical University Munich, Germany

ARTICLE INFO

Available online 13 January 2011

Keywords:
Fluid–structure interaction
Wind simulation
Real-scale test
Validation
Membrane structures

ABSTRACT

The sensitivity of membrane structures to wind loads due to their flexibility and small inertial masses raises the question of their behavior under natural wind conditions. Particularly transient wind loads could lead to dynamic amplification of the structural response. The assessment of the dynamic response of membrane structures is complex due to their special load carrying behavior, their material properties, and their distinct structural interaction with flow induced effects. Computationally intensive fluid–structure interaction simulation could overcome simplifications and limitations of existing approaches, especially small scale wind tunnel tests, and allow the assessment of all relevant structural and fluid phenomena. This paper outlines a virtual design methodology for lightweight flexible membrane structures under the impact of fluctuating wind loads and provides results on the unique validation of the method at real-scale tests of a highly flexible 29 m umbrella.

1. Motivation and background

1.1. Design of lightweight large umbrella structures in natural wind flow

The Architectural Office Rasch+Bradatsch is specialized in the architectural and structural design of lightweight structures. One of the major tasks during the last years was the design of convertible umbrella structures made of textile membranes and high strength steel (see Fig. 1). One challenge in the design of these highly flexible and extremely light structures is their sensitivity to wind-induced effects. Aero-elastic phenomena, such as dynamic buffeting, galloping and flutter, must be analyzed to guarantee a safe structural layout.

Mainly due to the extremely small thickness of the membrane, the application of well-established physical wind tunnel tests on small models is problematic. The inherent scale effects cause significant discrepancies of the measurements at simplified models and the real-scale structure's behavior. Moreover, a problem occurs in small scale wind tunnel tests, when large deformations of thin membranes interact with the fluid flow, because similarity conditions of both, the flow and the structural vibrations, are difficult to match. Small thickness dimensions of the membrane and large structural deformation under wind loads can be accommodated more readily in numerical simulations.

These issues, together with the need for a flexible tool to deal with complex geometries of varying structural concepts, motivated the formulation of an alternative, fully computational approach. During a series of engineering studies a numerical fluid–structure interaction (FSI) design methodology has been developed to investigate wind-induced effects on membrane structures (Michalski, 2009, 2007).

The final aim of these investigations is to apply the numerical method for the design of highly flexible, lightweight membrane structures in future projects. One important aspect of the numerical methodology is to create a wind field as input boundary condition for FSI simulation, which represents the previously determined statistical properties of the wind measurements at test site with sufficient accuracy. Therefore, one part of this contribution is the description of the integrated computational environment with an emphasis on the synthetic wind field generation.

1.2. Physical significance of numerical simulation

Little research has been done at the numerical investigation of the dynamic behavior of pre-stressed, double curved

* Corresponding author.
E-mail addresses: michalski@sl-rasch.de (A. Michalski), pdk@esi-group.com (P.D. Kermel), eberhard.haug@esi-group.com (E. Haug), rlohner@gmu.edu (R. Löhner), wuechner@bv.tum.de (R. Wüchner), kub@bv.tum.de (K.-U. Bletzinger).

0167-6105/$ - see front matter © 2010 Elsevier Ltd. All rights reserved.
doi:10.1016/j.jweia.2010.12.010

Fig. 1. Medinah Piazza Shading Project, 26 m umbrella, Medinah, Saudi Arabia 2010.

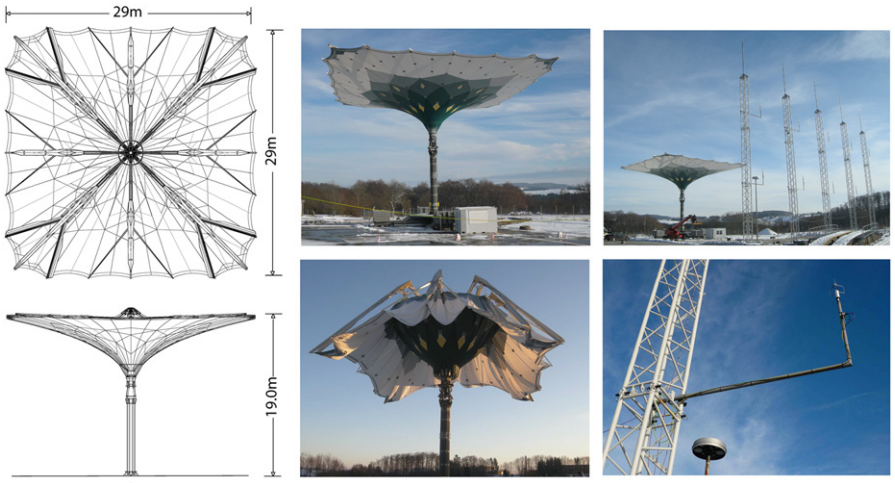

Fig. 2. 29 m umbrella (left, middle), wind measurement setup on test site of the company Liebherr (right).

membrane structures subjected to transient wind effects. Numerical simulation results were verified against wind tunnel tests of a conical membrane structure in nearly laminar flows (Glück, 2003; Kaiser, 2004). The structural behavior of air supported structures subjected to wind loads was evaluated in Kawamura and Kiuchi (1986), Kind (1984) and Newman and Ganguli (1984), where the flutter behavior of uniaxial curved hanging roofs was theoretically assessed in Kunieda (1975), Kimoto and Kawamura (1983) and Rosemeier (2008).

To evaluate the potentials and problems and to substantiate the acceptance of the numerical methodology, a real-scale test for the purpose of validation was set up. The validation of this highly complex multi-physics simulation relates to modeling aspects and possible sources of errors in the computation: the model error and the numerical error. The first one relates to the idealization of reality by a certain set of governing equations whereas the second one relates to the solution procedure for the discretized problem.

For validation, the complete simulation error is checked against the measured data of the full-scale test, which themselves contain also errors e.g. due to temperature influences, long term measurement, installation quality, etc. The consortium formed by the company Liebherr (manufacturers) the Architectural Office Rasch+Bradatsch (design) and ESI France (simulation) decided to validate the numerical methodology with an instrumented 29 m highly flexible umbrella prototype in an open wind-exposed area in southern Germany (Münsingen) (Fig. 2). In the simulations, the umbrella had to be modeled in the same environment and loaded by statistical wind data derived from the measured in situ wind data, transformed into corresponding synthetic turbulent wind time history inputs to the Computational Fluid Dynamics (CFD) software package (PAM-Flow, ESI Group). The structural response in the fully coupled FSI simulations was then compared to the measured response of the umbrella structure. This project constitutes a unique opportunity to validate the FSI simulation suite on a fully deformable 1:1 scale measured prototype structure.

2. Numerical methodology

The simulation methodology, consisting of the numerical wind flow simulation and the fluid–structure coupling simulation, is applied to determine the dynamic structural response of a 29 m umbrella under wind load. With this simulation approach, it is possible to examine all aspects of wind-loaded membrane structures, including aerodynamic and/or structural damping and the detection of aero-elastic effects. The applied FSI simulation methodology allows the realistic description of the nonlinear structural behavior at real-scale, which is especially important in the case of textile structures, and of the stochastic wind excitation, as both phenomena are modeled in time domain. The unknown parameters of the flow (velocity and pressure) as well as the structure (forces and deformations) are calculated including the fluid–structure coupling conditions. In this paper, the partitioned FSI solution approach realized in the commercial PAM software environment of the company ESI Group, Paris, is applied and extended by a preprocessing tool to generate synthetic wind flow fields with natural wind turbulence (NatWind). Fig. 3 shows the software components of the simulation methodology. This fully partitioned approach guarantees a maximum flexibility in software and hence allows for each subtask

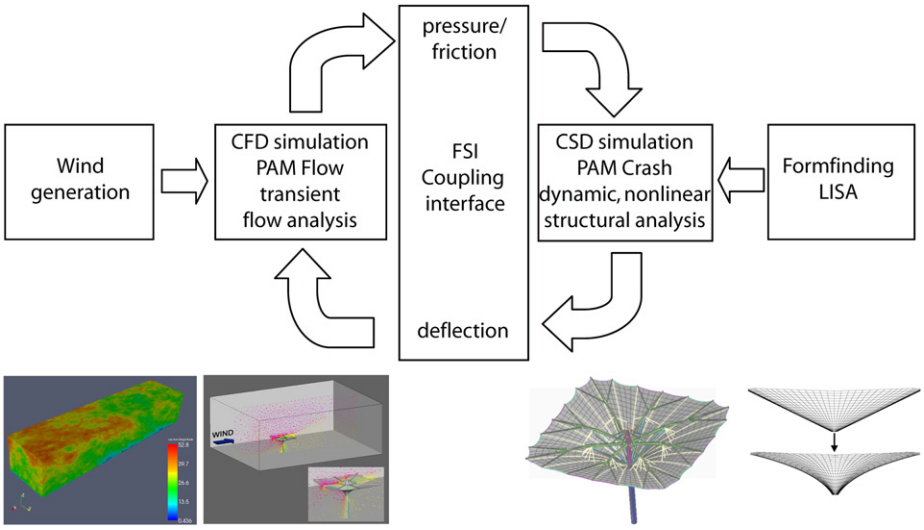

Fig. 3. Numerical simulation environment using a fully partitioned FSI approach.

the use of the best-suited and already tested solution schemes with their own discretizations.

2.1. Form-finding

Textile structures have, in comparison to conventional structures, a special structural behavior: due to their inability to withstand compressive forces and out of plane bending, their overall shape is coupled to their internal in-plane membrane stress state. Therefore their design is characterized primarily by defining the pre-stress and curvature conditions which determine the structural stiffness (Wüchner and Bletzinger, 2005). The definition of these properties has a crucial effect on the structural performance under wind loading. For this reason, shape finding has to be integrated in the numerical simulation process (Wüchner, 2006; Wüchner et al., 2007). In case of a newly chosen design or for necessary design changes, it is always the first step to compute a shape where the membrane is in equilibrium with the introduced pre-stress, geometric boundary conditions and loads, which is then the basis for the simulation of the FSI problem (Bletzinger et al., 2010, 2009, 2005; Bletzinger and Ramm, 1999; Schek, 1974; Barnes, 1994). The software used in this contribution is Lightweight Structure Analysis (LISA), an implicit 3D nonlinear finite element tool which uses an iterative implicit FEM approach with modified Newton–Raphson iteration to converge towards pre-stress controlled membrane shapes (Haug and Powell, 1972; Haug et al., 2009, 1991; Haug and de Rouvray, 1984; Haug, 1972, 1988)).

2.2. Computational Fluid Dynamics (CFD)

For the treatment of incompressible flows, the CFD software PAM-Flow of ESI Group is applied. PAM-Flow is a general-purpose CFD code based on the following principles:

- use of unstructured grids (automatic grid generation and mesh refinement);
- finite element discretization of space (specialized to linear elements);
- separate flow modules for compressible and incompressible flows;
- ALE formulation for moving grids;
- edge-based data structures for speed and the use of limiting and upwinding;
- optimal data structures for different architectures;
- bottom-up coding from the subroutine level to assure an open-ended, expandable architecture.

The equations solved are the Navier–Stokes equations describing an unsteady, incompressible flow, given by

$$\nabla\cdot\mathbf{v}=0$$
$$\rho\mathbf{v}_{,t}+\rho\mathbf{v}\cdot\nabla\mathbf{v}+\nabla p=\nabla\mu\nabla\mathbf{v}+\mathbf{f}+\rho\mathbf{g} \tag{1}$$

Here ρ, $\mathbf{v}$, p, μ and $\mathbf{g}$ denote, respectively, the density, velocity, pressure, viscosity and gravity vector, while $\mathbf{f}$ is the vector of external forces. The equations are advanced in time using the following projection-type solver:

a) *Advective-diffusive prediction*: $\mathbf{v}\rightarrow\mathbf{v}^*$

$$\left[\frac{\rho}{\Delta t}-\theta\nabla\mu\nabla\right](\mathbf{v}^*-\mathbf{v}^n)+\rho\mathbf{v}^n\cdot\nabla\mathbf{v}^n+\nabla p^n=\nabla\mu\nabla\mathbf{v}^n \tag{2}$$

b) *Pressure correction*: $p^n\rightarrow p^{n+1}$

$$\nabla\cdot\mathbf{v}^{n+1}=0$$
$$\frac{\mathbf{v}^{n+1}-\mathbf{v}^*}{\Delta t}+\frac{1}{\rho}\nabla(p^{n+1}-p^n)=0$$
$$\Rightarrow -\nabla\frac{1}{\rho}\nabla(p^{n+1}-p^n)=\frac{\nabla\cdot\mathbf{v}^*}{\Delta t} \tag{3}$$

c) *Velocity correction*: $\mathbf{v}^*\rightarrow\mathbf{v}^{n+1}$

$$\mathbf{v}^{n+1}=\mathbf{v}^*-\frac{\Delta t}{\rho}\nabla(p^{n+1}-p^n) \tag{4}$$

Note that at steady state flow conditions, the residuals of the pressure correction vanish, implying that the result does not depend on the time step Δt. The usual difficulties associated with the first-order spatial difference operators are treated via limiting and upwinding for the advection operator (Löhner, 2008) and 4th order damping for the divergence constraint (Löhner, 2004; Löhner et al., 2006). One can improve the temporal accuracy of the advection-diffusion operator using explicit Runge–Kutta substepping schemes (Löhner, 2004). For the present calculations, a 5-stage scheme was employed. The pressure-equation is solved using deflated diagonally preconditioned conjugate gradient algorithms (Aubry et al., 2008) with projective pressure prediction (Löhner, 2005). For the modeling of turbulent flows, a large eddy

simulation (LES) model based on the Smagorinsky subgrid scale (SGS) model is used. For the coupling with a structural simulation the fluid calculation is performed on moving meshes (ALE description). Typically, no more than 30 layers of elements surrounding the moving parts are allowed to move using a Laplacian-based velocity smoothing technique (Löhner, 1993). Should any of these moving elements become too deformed in the course of the simulation, PAM-Flow proceeds as follows: the deformed elements (and 1–2 neighboring layers) are removed, the regions are remeshed, the solution is reinterpolated, and the simulation continues. PAM-Flow has been ported to vector, shared memory parallel via OpenMP (Löhner, 1998) and distributed memory parallel machines where the code communicates via MPI (message passing interface).

2.3. Computational Structural Dynamics (CSD)

Due to their high flexibility, the considered umbrella structures exhibit large deformations under dynamic wind action. This necessitates a fully geometrically nonlinear formulation of the structural elements with a solution scheme in time domain. Within this project, beam, cable, membrane and shell elements are used to model the solid parts. Particularly, the complex material behavior of textile membranes has to be modeled by a specific orthotropic constitutive law.

Within this project, a general version of the Computational Structural Dynamics (CSD) analysis code PAM-Crash is chosen as dynamic structural simulation software for its advanced capacities. This finite element code is best known from car crash and membrane airbag simulation, and can be used for the dynamic and quasi-static simulation of any type of solid body or structure. In particular, this code is well suited to perform ultimate load rupture/failure analysis of the steel skeleton and of the membranes. Moreover, its sophisticated contact algorithms allow a detailed simulation of partially folded umbrellas, where the slackened membrane can undergo self-contact and contact with the steel structure under gravity and wind loads. It is based on an explicit 3D finite element formulation, specifically designed for the simulation of transient, nonlinear response of large and complex structures (Haug, 1981; Haug et al., 1986).

2.4. Fluid–Structure Interaction (FSI)

The coupling of CFD and CSD codes for FSI calculation is realized via a partitioned approach in an explicit manner (Löhner et al., 1994, 1995). The methodology allows the use of different time steps in the fluid and structural parts for a given simulated physical duration, using sub-cycling. Information is updated at each time step for each solver (by interpolation) so that transient simulations are very easily achieved. The flow solver passes the surface loads (pressures, shear stresses) to the structure, while the structural solver passes the surface location and velocity to the flow domain. Fast interpolation and projection techniques (Cebral and Löhner, 1997a, 1997b) are used to ensure that the extra CPU requirements due to a coupled simulation are kept to a minimum.

The coupling conditions apply to both sides of the thin membrane, which are provided each with refined 2D surface grids connecting to the 3D CFD mesh. These grids are used to interpolate the pressures calculated in the fluid domain onto the finite element nodes of the structural model of the thin membrane. The CSD mesh density is the same as in an uncoupled CSD model. The mesh densities used on both sides of the membrane of the CFD field are identical and determined mainly from geometrical considerations (curvature, proximity of other structural parts). The interpolations required in the coupling algorithm are based on the element shape functions; loads are assembled as forces at the CFD nodes along the coupled interface, then the forces are distributed using the shape functions at the CSD nodes of the corresponding CSD element. A similar process is used for displacements.

At the fluid–structure interface a no flux boundary condition is applied. This allows along the smooth surface only tangential velocity to the surface. In addition, a law of the wall is used to include friction effects.

2.5. Wind simulation

Atmospheric boundary layer wind fluctuations are generated synthetically and applied at the inflow section of the LES solver by a specific wind module (NatWind), which is interfaced to the CFD software PAM-Flow. Due to the fact, that it is nearly impossible to determine spatial and time dependent wind velocity fields from measurements, synthetic input wind velocity fields could be generated from known statistical wind data (Deodatis and Shinozuka, 1991; Rossi, 2004; Shinozuka and Jan, 1972).

It is assumed that "wind" is a stationary ergodic gaussian stochastic process, where the statistical quantities are time-independent and can be extracted from any available wind record. The wind velocity field is composed from a mean wind speed profile by adding the generated fluctuating components.

Within a preprocessing step, time and space correlated "frozen" wind fields are generated based on the processing of statistical meteorological data. The velocity vectors are computed for a spatial field with side lengths of L_i with $i=1, 2, 3$, and $N_1 \times N_2 \times N_3$ grid points and a grid space of $\Delta L_i = L_i/N_i$ (see Fig. 7a). With the help of Taylor's hypothesis the spatial velocity field is transformed into time series for the application at the inflow section of a CFD simulation. For detailed information refer to Mann (1994,1998) and Michalski (2010). The fluctuating components are realized more specifically by a three-dimensional fast Fourier transformation (FFT) technique in wave number space, where the atmospheric surface layer turbulence is based on spectral tensors. This method has been developed by Mann (1998) and realized in the context of the generation of wind flow for FSI simulation for lightweight structures by Michalski (2010).

The fluctuating velocity vector is calculated using a three-dimensional inverse FFT:

$$u_i(\mathbf{x}) = \sum_{\vec{k}} e^{i\mathrm{kx}} C_{ij}(\mathbf{k}) \cdot n_j(\mathbf{k}) \tag{5}$$

Including the ith component of the velocity vector $\mathbf{u}(x)=\mathbf{u}(x, y, z)=[u_1(x, y, z), u_2(x, y, z), u_3(x, y, z)]^{\mathrm{T}}=[u(x, y, z), v(x, y, z), w(x, y, z)]^{\mathrm{T}}$. The coordinates of the spatial grid points are obtained by $x_l = N_l \Delta L_l$ with $l=1, \ldots, 3$. N_l is the number of grid points of the lth component of the vector $\mathbf{x}$. The symbol Σ describes the sum over all wave number vectors $\mathbf{k}=[k_1, k_2, k_3]^{\mathrm{T}}$ with the components $k_i = m2\pi/L_i$ with $i=1, 2, 3$ where m takes integer values of $m=-N_i/2, \ldots, N_i/2$. $n_j(k)$ are complex Gaussian random numbers with a variance of 1 and a mean of 0. The coefficient C_{ij} is determined by the decomposition of the spectral tensor for atmospheric surface layer turbulence developed by Mann. The tensor contains essential aspects of the second-order structure of atmospheric turbulence, i.e. negative correlation coefficients $\rho_{uw} < 0$ and ratios of variances $\sigma_u^2 > \sigma_v^2 > \sigma_w^2$ with $\sigma_w^2/\sigma_u^2 = 0,\ 25$ and $\sigma_v^2/\sigma_u^2 = 0.5$–$0.7$, spectra and coherence functions. The sheared spectral tensor in its factorized form is given by

$$C_{ij}(\mathbf{k}_0) = (\Delta k_1 \cdot \Delta k_2 \cdot \Delta k_3)^{1/2} \cdot A_{ij}(\mathbf{k}_0) \tag{6}$$

with

$$A_{ij}(\mathbf{k}_0)=\frac{\sqrt{E(k_0)}}{\sqrt{4\pi}{k_0}^2}\begin{bmatrix} k_2\zeta_1 & k_{30}-k_1\zeta_1 & -k_2 \\ -k_{30}+k_2\zeta_2 & k_1\zeta_2 & k_1 \\ k_2k_0^2/k^2 & -k_1k_0^2/k^2 & 0 \end{bmatrix} \tag{7}$$

where the energy spectrum, $E(k)$, is chosen to be (as suggested by V. Kármán):

$$E(k)=\alpha\varepsilon^{2/3}L^{5/3}\frac{L^4k^4}{(1+L^2k^2)^{17/6}} \tag{8}$$

with the parameters L (length scale) and $\alpha\varepsilon^{2/3}$ where α is the Kolmogorov constant and ε the rate of viscous dissipation of specific turbulent kinetic energy.

The coefficient matrix A_{ij} includes with $k_0=[k_1,\ k_2,\ k_{30}]^{\mathrm{T}}=[k_1,\ k_2,\ k_3+\beta(k)k_1]^{\mathrm{T}}$ and $k_0=(k_1^2+k_2^2+k_3^2)^{1/2}$ the following parameters:

$$\zeta_1=C_1-\frac{k_2C_2}{k_1}\quad \zeta_2=\frac{k_2C_1}{k_1}+C_2 \tag{9}$$

with

$$C_1=\frac{\beta k_1^2(k_0^2-2k_{30}^2+\beta k_1k_{30})}{k^2(k_1^2+k_2^2)} \tag{10}$$

and

$$C_2=\frac{k_2^2k_0^2}{(k_1^2+k_2^2)^{3/2}}\arctan\left[\frac{\beta k_1(k_1^2+k_2^2)^{1/2}}{k_0^2-k_{30}k_1\beta}\right] \tag{11}$$

where the dimensionless eddy lifetime β is

$$\beta(k)=\frac{\Gamma}{(kL)^{2/3}\sqrt{{}_2F^1((1/3),(17/6),(4/3),-(kL)^{-2})}} \tag{12}$$

with the hypergeometric function F (Vetterling et al., 2001) and a parameter Γ. Within this study, parameters of the sheared spectral tensor, fitted to the Kaimal spectra from literature, were used. Γ was set to 3.9, whereas L was set to $L=0.95z$ with $z=25$ m and

$$\alpha\varepsilon^{2/3}=\frac{3.2u^*}{z^{2/3}} \tag{13}$$

with the friction velocity of $u^*=1.1$ m/s.

The effect of the mean shear of the flow on the turbulence is modeled with the concept of eddy lifetimes. The result of this approach is that the turbulent field described initially by the isotropic von Karman tensor will become anisotropic, which leads then to the sheared spectral tensor for surface layer turbulence. Details of the derivation of the sheared spectral tensor and the quality of the physically modeling, the calibration, etc. could be found in J. Mann.

It is necessary to provide for each grid point of inflow section of the CFD domain, information on the time-resolved turbulent fluctuations of the numerical flow simulation. These transient unsteady boundary conditions are computed within a separate wind simulation environment on a fixed Cartesian "wind" grid. Subsequently, the wind data is applied at the inflow section of the CFD simulation, interpolated in space (bicubic) and time (linear) and passed to the CFD computational grid.

3. Real-scale field test

3.1. Setup and measurement model

An experimental setup was implemented at a test site of the company Liebherr in which both the aerodynamic behavior of the 29 m umbrella in atmospheric wind flow and the upstream located wind field were measured simultaneously, resolved spatially and temporally (Fig. 2).

The system responses of the umbrella mast, the middle, diagonal and passive arms of the 29 m umbrella (specific weight of the membrane is 1 kg/m^2) and their respective correlation to the loading process were measured using 76 strain gauges (Fig. 4, right) simultaneously with the wind field.

Moreover, a photogrammetric method has been applied to capture the full three-dimensional, time-resolved membrane movement (Fig. 4, left). In this type of measurement systems, the reconstruction of moving spatial objects is obtained from the photographs. This procedure was implemented using four cameras that were positioned in front of the umbrella, tracing the moving umbrella simultaneously.

The objective to reproduce numerically the dynamic response of a membrane structure exposed to turbulent wind flow as close

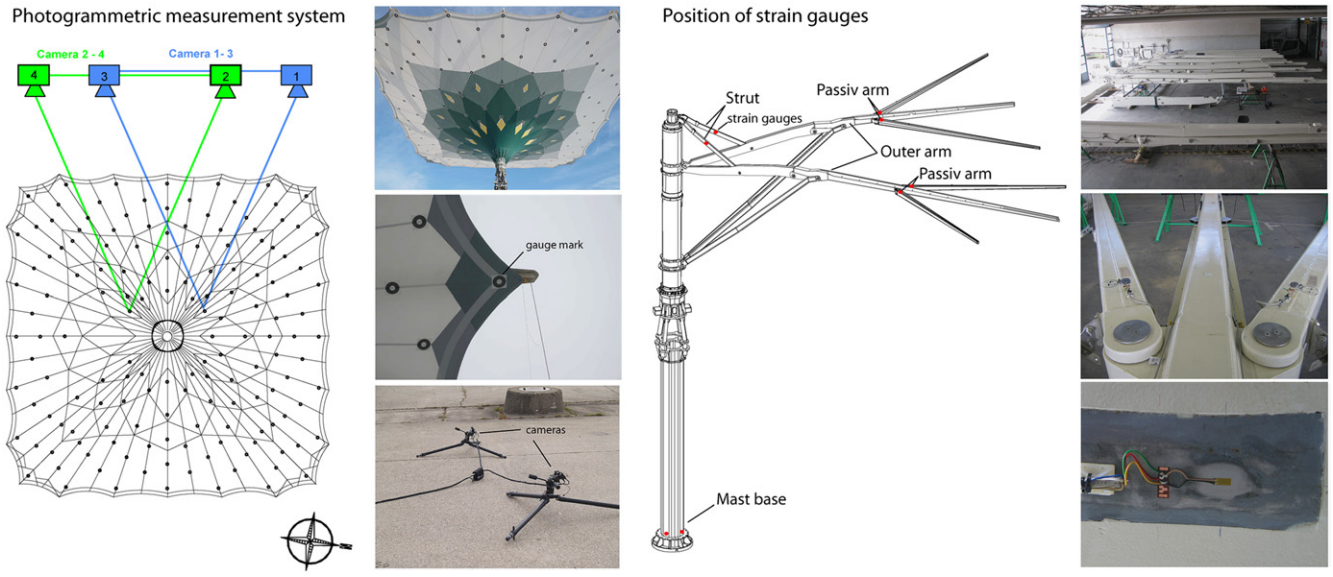

Fig. 4. Photogrammetric deformation measurement system: floor cameras and optical gauge points (left), strain measurement at the steel structure: steel skeleton segment and strain gauge locations (right).

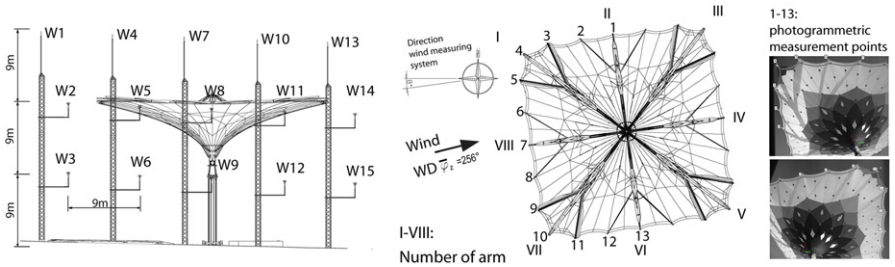

Fig. 5. In situ wind measurements on 1:1 prototype umbrella (left: anemometer locations, center: arm numbers for strain and deflection measurement).

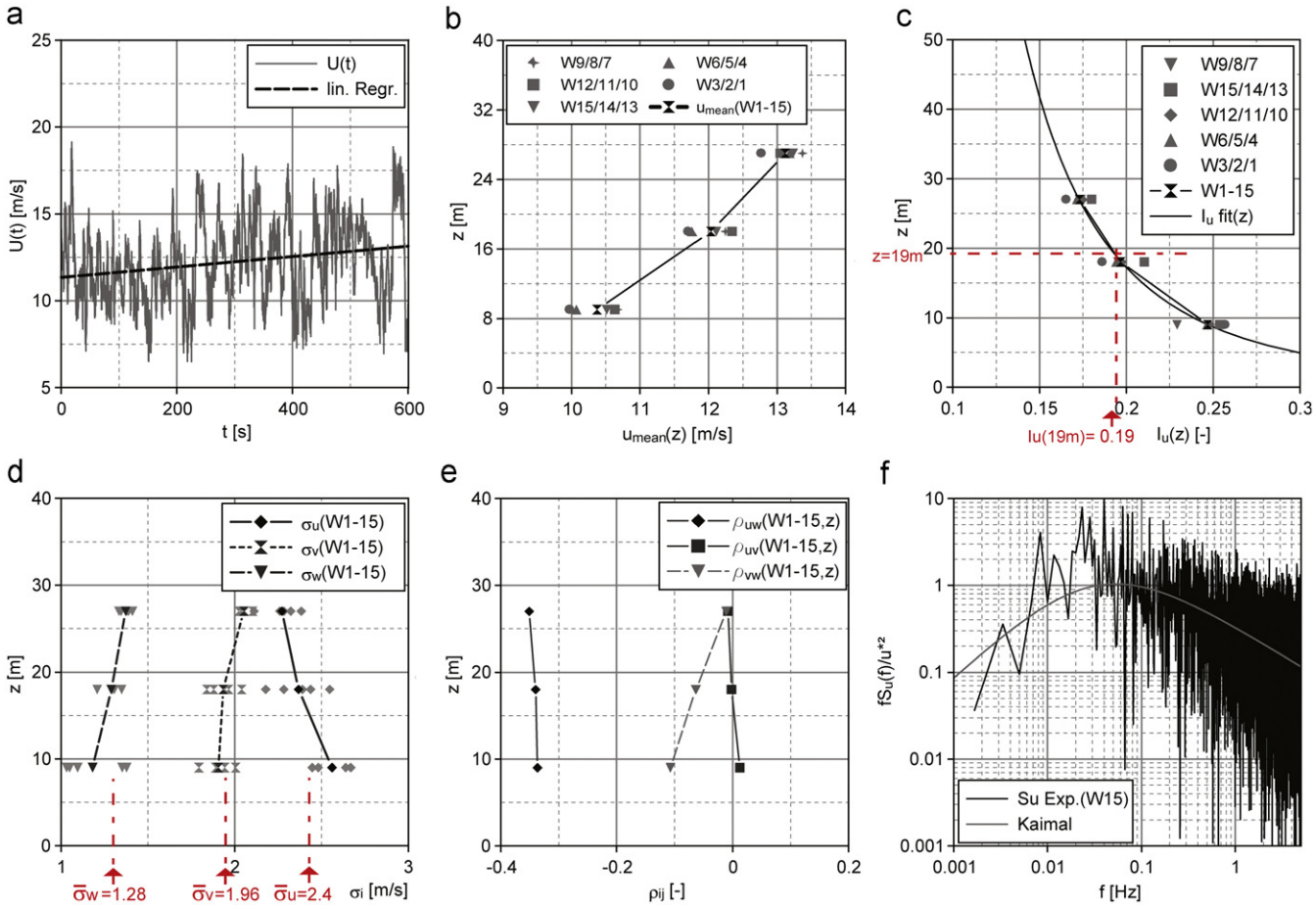

Fig. 6. Statistical wind data of the selected event: (a) target wind record; (b) mean wind speed; (c) turbulence intensity; (d) standard deviation of velocity components; (e) correlation coefficient; and (f) spectral density distribution.

to reality as possible, requires precise knowledge of the wind field in upstream direction of the umbrella. As simple mechanical measuring devices like cup anemometers are unable to meet the necessary requirements, sonic anemometers of Young type have been used to measure the wind field (Fig. 2, right, Fig. 5, left). Five masts in a grid spacing of 9 m were installed where the entire three-dimensional wind vector, i.e. the wind speed and direction, was measured at 15 positions.

The sample rate of the entire measurement system including the wind speed, the steel strain and membrane deformation was 10 Hz. The measurement uncertainty of the strain measurements was estimated to be around 5% due to influences of temperature, long term measurement of the in situ measurement setup, opening and closing of the umbrella, etc. The accuracy of the wind measurement with the sonic anemometers is about 1% at wind speeds from 0–30 m/s. The accuracy of the photogrammetric system is determined in preliminary tests to be around 1% at displacements up to 20 cm. The complete measurement setup was checked by independent wind engineering experts (Windtest Grevenbroich GmbH) regarding the functionality and quality of the system including the measurement hardware, connections of the measurement devices, etc.

3.2. Evaluation of the experimental wind speed measurements

The whole measurement system was installed from the beginning of November 2008 to the end of February 2009. Within this period, 90 measurement periods were recorded, triggered by wind speeds greater than 6 m/s, with a length of 10 min each. To perform the desired comparison of the experimentally determined reaction forces and deformations with results of numerical simulations, the real wind field acting on the umbrella has to be

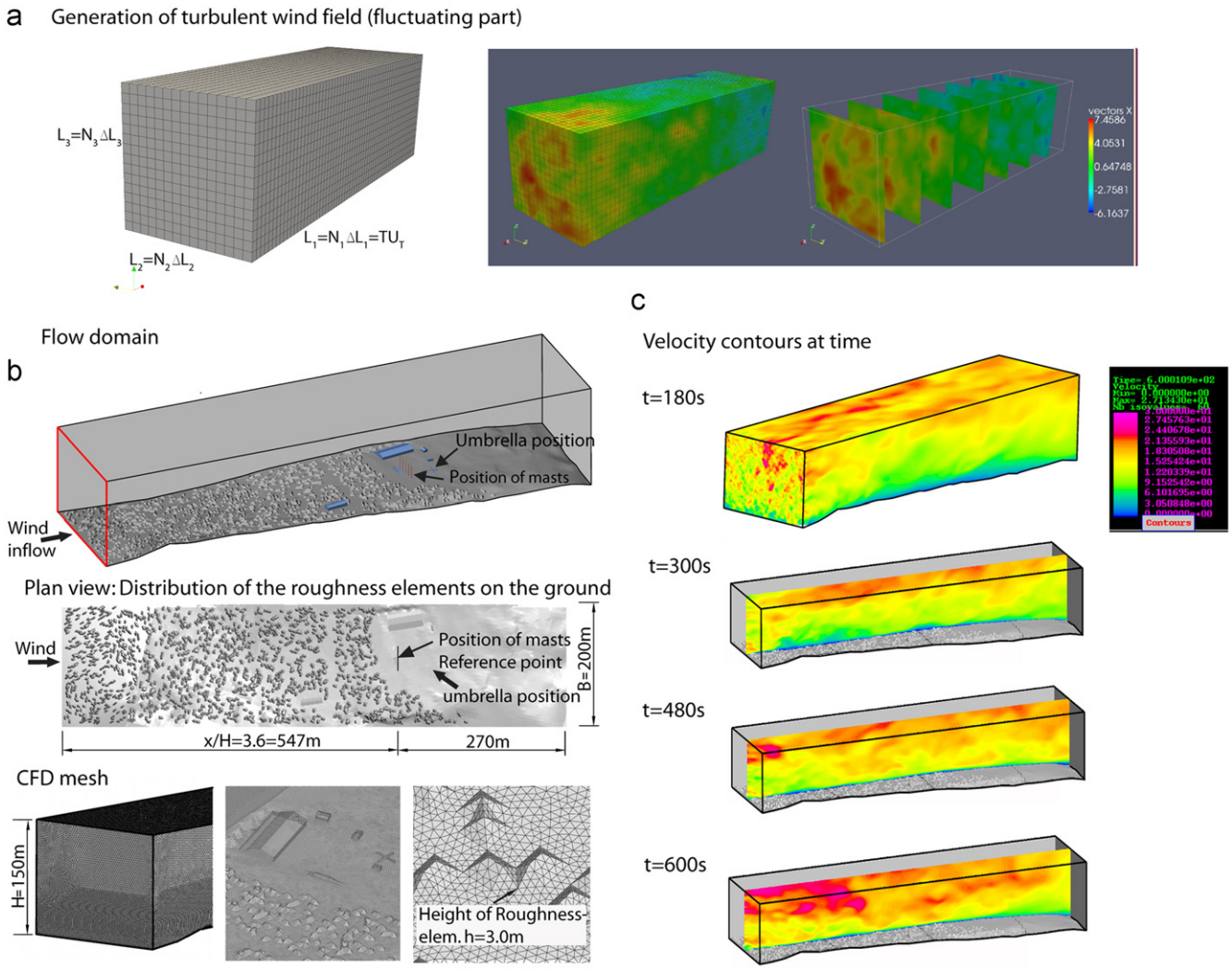

Fig. 7. CFD simulation with a long inflow length: (a) generated "frozen" wind field; (b) flow domain; and (c) velocity contour snapshots at different times on the domain boundaries (180 s) and in a longitudinal-vertical cut plane.

reproduced artificially in its main statistical properties and assigned to the numerical flow simulation as inflow conditions. Therefore the measured wind data has to be evaluated.

In the following, the analysis of wind data is exemplarily described for one single record. The corresponding wind event took place on 10 February 2009, with a maximum gust wind speed of 20 m/s in 18 m height. This measured wind field is the target for the numerical wind field generation.

The average wind direction of all 15 sonic anemometers relative to the orientation of the measurement masts is -5.86° and lies within the defined limits. Fig. 6a shows the time history of the wind speed at measurement point W8 and the time-averaged and spatially span-wise averaged wind speeds at the sonic anemometers in the heights of 9, 18 and 27 m of the five masts (Fig. 6b).

Applying a curve fitting, the profile exponent α can be determined to $\alpha=0.21$ and the reference speed to $u_{\mathrm{ref}}\,(10\,\mathrm{m})=10.61$ m/s. The standard deviations of the turbulence components σ_u, σ_v and σ_w at all measurement points are plotted over height z and averaged in span-wise direction (Fig. 6d). The evaluation of the mean values (solid lines) in the heights of 9, 18 and 27 m shows that components in lateral and vertical direction are behind those of the longitudinal direction. The turbulence intensity, defined as $T(z)=\sigma(z)/\overline{u}(z)$, at the at height of the membrane edge is approximately 19% (see Fig. 6c), where σ is the standard deviation and $\overline{u}$ is the mean velocity at height z. The correlation coefficients of the longitudinal and vertical fluctuation component is $\rho_{uw}=-0.35$ (Fig. 6e). The evaluation of the spectral curves of all velocity components at the test site shows a very good agreement with the Kaimal spectrum (Fig. 6f). It could be concluded, that the measured wind data satisfies the requirements for the synthetic wind modeling procedure outlined in Section 2. The selected strong wind of 10 min duration has been modeled within the CFD simulation. The time averaged lift force at the mast base of the umbrella due to wind is measured to be 14 kN, the mass of the membrane 8.1 kN. The stiffness (EA) of the membrane is 1000 kN.

4. Comparison of simulation results with real-scale measurements

The described specific wind field with duration of 10 min is generated numerically, considering its essential properties in two different flow simulations. Since the measurement setup could only be installed for a limited period within this industrial project, only one wind condition was investigated. Results of the CFD simulation and the following FSI simulation are described within this section. Fig. 5 shows the in situ wind measurements on

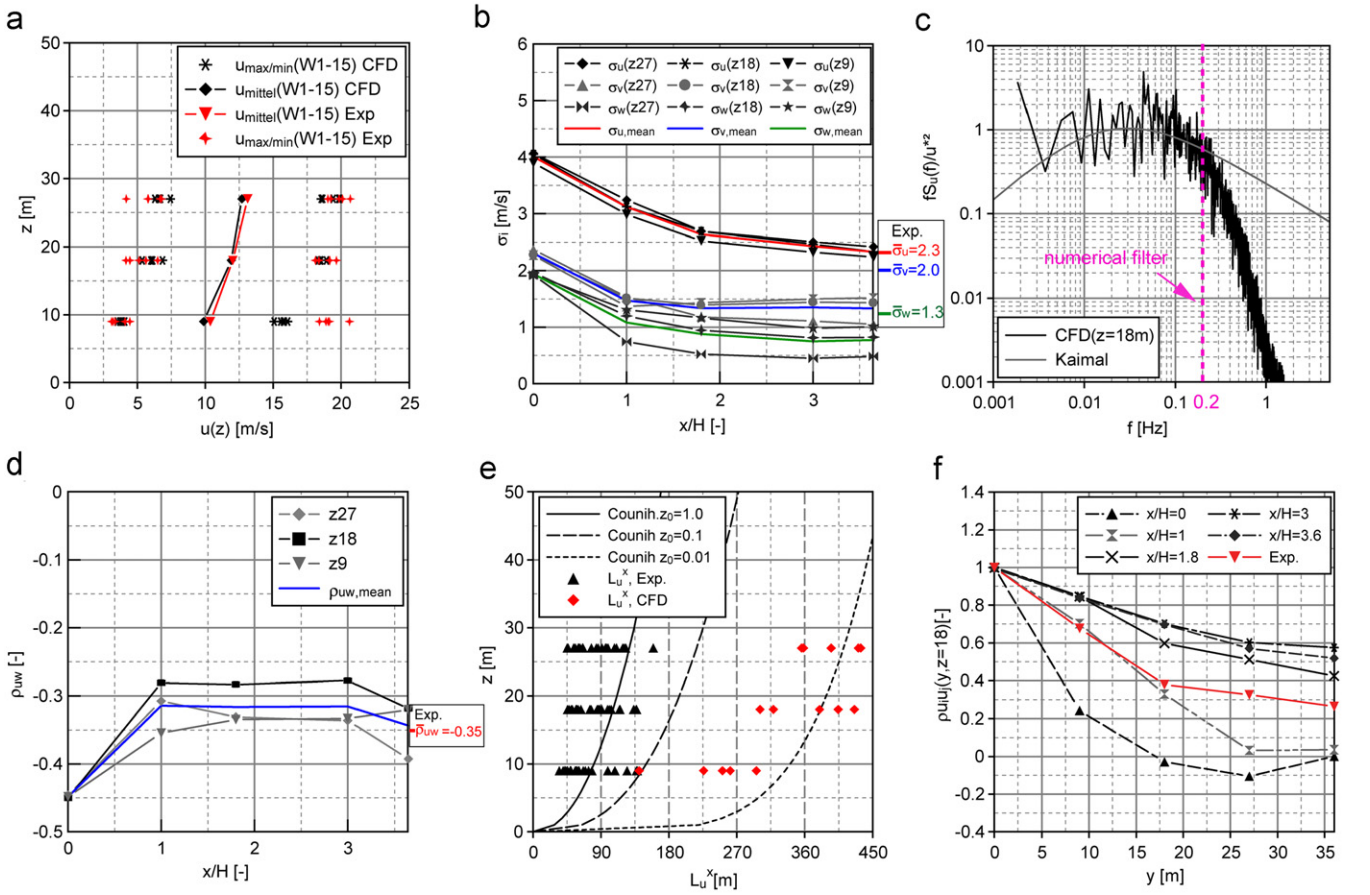

Fig. 8. Comparison of statistical wind data of LES simulation with a long inflow length (synthetic wind field applied at inflow section) with results from measured data: (a) mean and gust wind speeds; (b) standard deviation of the velocity components; (c) spectral density distribution; (d) correlation coefficient; (e) integral length scales; and (f) cross correlation coefficient.

the 1:1 prototype umbrella as well as the numberings of the umbrella arms, measurement positions of the photogrammetric measurement system.

First the results of a simulation with an ideal long inflow length including roughness elements is described, followed by a description of the results of a simulation with a shorter inflow length. In both simulations, unsteady inflow boundary conditions (generated with NatWind) are applied. However, for the long and small channel a different set of inflow boundary is applied in order to get comparable flow characteristics to the experiment. The first simulation was not considered conclusive, mainly due to the lack of available compute power, which could not accommodate the required element density of the long CFD domain. Therefore a second analysis was performed, using a higher element density over a shorter inflow domain length, which greatly improved the results.

In general, the performed studies permit the following observations:

- Long inflow domains improve the downwind stability of the simulated atmospheric boundary layer, but increase the effect of numerical dissipation in the higher frequency range of the energy spectra, which can only be overcome by increasing the mesh density in the CFD domain. This leads to high CPU times, which can become prohibitive.
- Shortening of the inflow domain reduces CPU requirements and numerical dissipation at the same CFD mesh density. At higher mesh densities it further reduces numerical dissipation. However, the atmospheric boundary layer may not have reached downwind stability, which is acceptable when the generated flow reach correctly the target wind characteristics in the neighborhood of the wind-loaded object. The quality of the wind inflow conditions compared with the natural wind flow, generated with NatWind becomes more important.

4.1. Simulation with a long inflow length including roughness elements

The model features of the flow domain and of the umbrella structure are described in this section for both, the long and short inflow domain simulations. The objective for the choice of a long inflow section was to obtain 'model-consistent' turbulence at the reference position (position of the masts, see Fig. 7b), based on the fact that a synthetic turbulent wind field was applied at the inflow section. An equilibrium boundary layer should be obtained.

4.1.1. CFD simulation

In order to show that the natural wind flow could be reproduced with sufficient accuracy by CFD analysis, simulations on the empty channel were performed first. The domain of the empty channel flow simulations is shown in Fig. 7b. It includes the terrain profile at the measuring site with geometric obstacles (buildings) and in addition geometric roughness elements ("bumps"). These elements are randomly distributed and were introduced in order to maintain the introduced turbulent boundary layer, especially vertical turbulence.

The measured wind data of Fig. 6 are now reproduced by a synthetic wind field, generated according to the methods described in Michalski (2010). Fig. 7a shows the spatial turbulent wind field

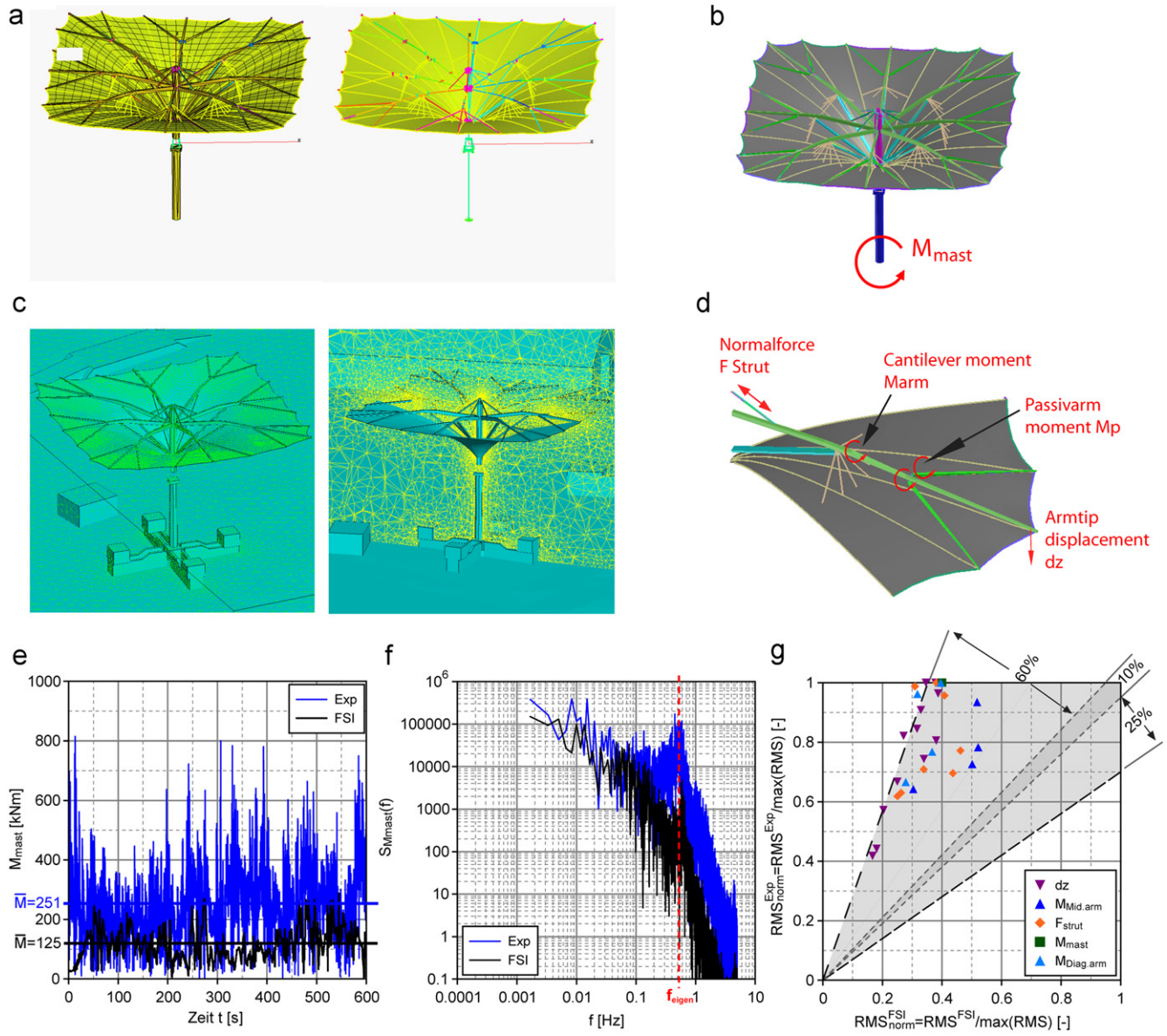

Fig. 9. FSI simulation with a long inflow length: (a) CSD Model; (b) evaluation of mast foot moment; (c) CFD model and mesh; (d) evaluation of arm reactions; (e–g) comparison of simulation and measurement results; (e) time history mast foot moment; (f) spectral density distribution mast foot moment; and (g) normalized RMS values of umbrella response.

which is transferred into a temporal one and subsequently superimposed to a mean wind speed profile. The number of unstructured tetrahedral elements used is about 6 million. At the outflow, static pressure boundary conditions, and at the ground "no-slip" boundary conditions are used. On the outer boundaries, a special constant pressure, in- and outflow boundary conditions is applied which allows the fluid to leave and enter the domain (depending on the pressure conditions). The Reynolds number calculated with channel height as a reference length is $Re = 50 \times 10^6$. The modeling of the turbulence was performed with a LES approach using a Smagorinsky model ($Cs = 0.11$). This transient simulation ran with a time step of 0.15×10^{-1} s and a Runge–Kutta time integration scheme of 5th order with a CFL condition of 1.2. The simulation time for this task was approximately 70 h on a Linux cluster (Dual Opteron 252) with 50 processors.

The analysis of statistical parameters was carried out at the locations $x/H = 1, \ldots, 3.6$, with the channel height $H = 150$ m, each of which contained a total of 15 measurement positions on the heights of 9, 18 and 27 m. Statistical analysis was performed with a total of 36 000 time steps over 540 s. Fig. 8 contains comparisons of wind data derived from the in situ wind measurements with the same data determined from the simulation with the generated synthetic wind field. The simulation on the empty flow domain produced the following properties of the generated wind field: The extreme (min,max) and mean values $\overline{u}(z)$ of the velocity fluctuations at different anemometer locations (W1-15) agree with the experimental values (Fig. 8a).

Fig. 8b compares the values of the standard deviations σ_u, σ_v, $\sigma_w(x/H)$ of the wind field velocities with the experimental values along the (normalized) channel length, x/H, where constant values are reached after about $x/H = 1.5$. The drop in values along the channel's length direction is due to the fact that the channel flow must find its own equilibrium as dictated by properties of the numerical model. The differences are taken into account during calibration of the wind inflow model parameters. Compared to the in situ measurements, the vertical and lateral fluctuating components are underestimated. As can be seen in Fig. 8b, the equilibrium boundary layer is obtained at a distance of two to three

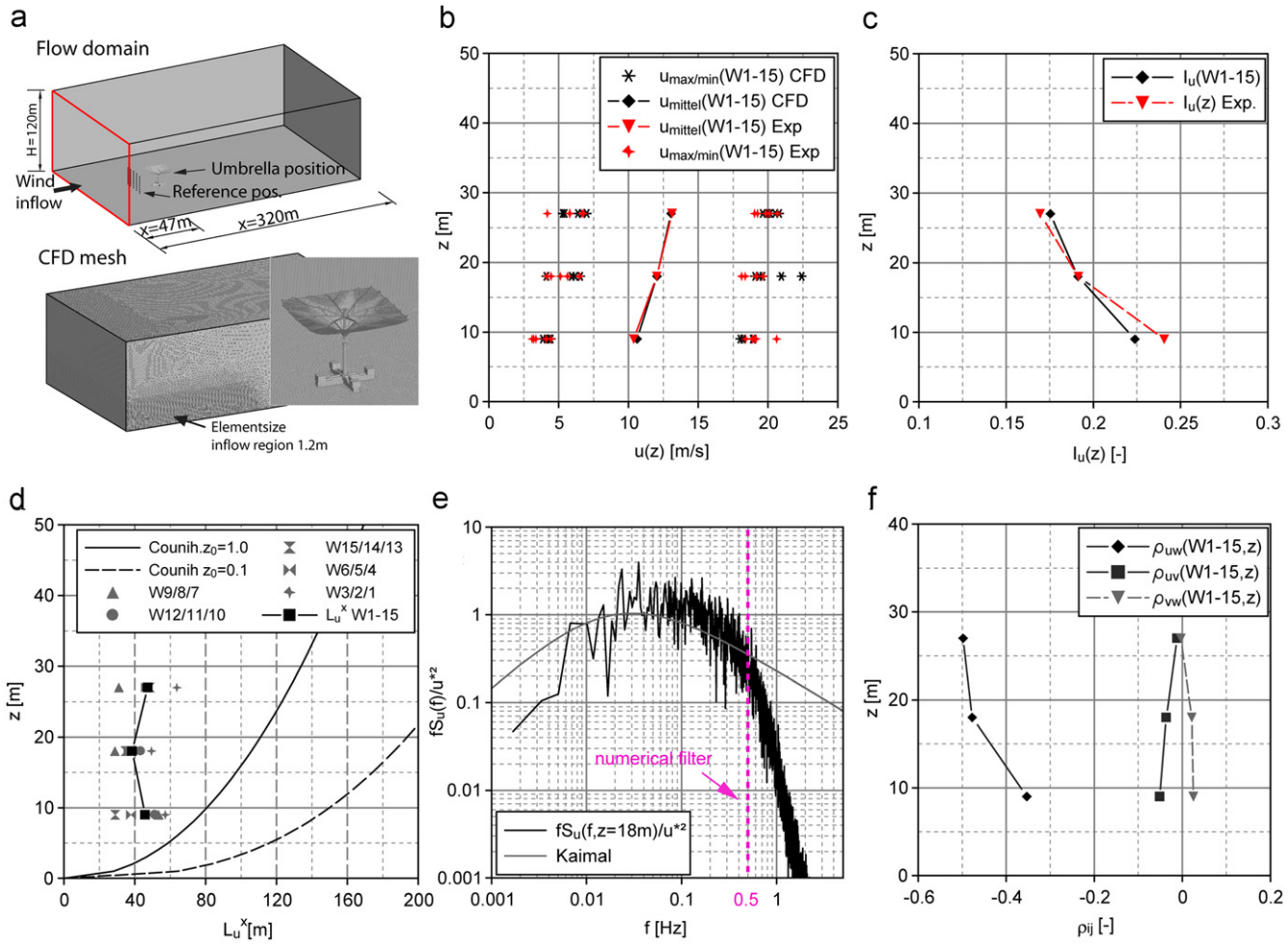

Fig. 10. Comparison of statistical wind data of LES simulation with a short inflow length (synthetic wind field applied at inflow section) with results from measured data: (a) flow domain; (b) mean and gust wind speeds; (c) turbulence intensity; (d) integral length scales; (e) spectral density distribution; and (f) cross correlation coefficient.

times the domain height. Fig. 8c shows the calculated normalized gust spectrum $fS_u(f)$ which agrees with the norm Kaimal spectra in the range of the lower frequencies. A drop in the upper frequency range occurs at approx 0.2 Hz which is a result of the spatial filtering of the LES simulation. The normalized correlation coefficient $\rho_{uw}(x/H)$ agrees well with the experimental values (Fig. 8d). The curves of the integral length scales (see Fig. 8e) in the different heights vary from the experimental results. They are in general higher than the strong-scattering measurements and are therefore conservative for wind load determination.

Fig. 8f, finally, compares cross correlation coefficients $\rho_{uiuj}(y)$ at different lengths x/H with the experimental results. By comparing the statistical parameters of the simulation with the field measurement at the reference position, it can be shown that the natural wind flow could be modeled for the FSI simulation with sufficient accuracy.

4.1.2. *Fluid–structure interaction simulation*

In this section, results of the numerical FSI simulations, carried out by the company ESI France, are presented. This requires the determination of the actual mechanical and dynamic behavior of the built prototype umbrella and to accurately calibrate the computational structural model, by taking into account discrepancies of the built umbrella from the planned state, arising for example by material, and manufacturing tolerances. To determine the dynamic behavior of the prototype, the mass, stiffness and damping characteristics of the steel structure, the cladding and the membrane had to be determined from preliminary experiments.

Fig. 9 shows the used CSD model which consists of a total of 6612 nodes, 1536 membranes, 4002 null shells for the coupling interface between the wetted surfaces, 648 cables and 493 beam finite elements. The CFD domain with 7 million tetrahedral elements of Section 4.1.1 was applied. Generated synthetic wind data (as prescribed in Section 2.5) have been injected into the PAM-FSI model and the simulation was running in MPI shared memory parallel (SMP) mode on parallel machines, where each code uses SMP execution and both codes communicate via MPI. The form-finding was performed using the software LISA and enters as a preprocessing step in the FSI simulation. The coupled simulation is running on a Linux cluster on eight processors (HP-Nehalem), where seven CPU are reserved for the CFD solution and one for the CSD solution. For 24 s simulated real time, the spent CPU wall clock time is about 24 h. The time step in PAM-Flow is about 5.0×10^{-3} s when a selected Runge–Kutta approach of 5th order and a CFL condition of 1.4 is applied. The ratio of CSD/CFD time steps in the sub-cycling iterations is 1:685.

In this study, the simulations starts with air at rest (velocity=0), then the unsteady inflow is applied gradually over a few ten seconds. During this startup phase of the FSI simulation, extra mass proportional damping is included to setup a steady flow regime and remove structural oscillations resulting of the sudden application of the self-weight and pre-stress. A short duration, compared to the full 10 min simulation, is used to get a state with balanced wind loads and internal stresses. During the main phase of the FSI simulation no structural damping is taken into account.

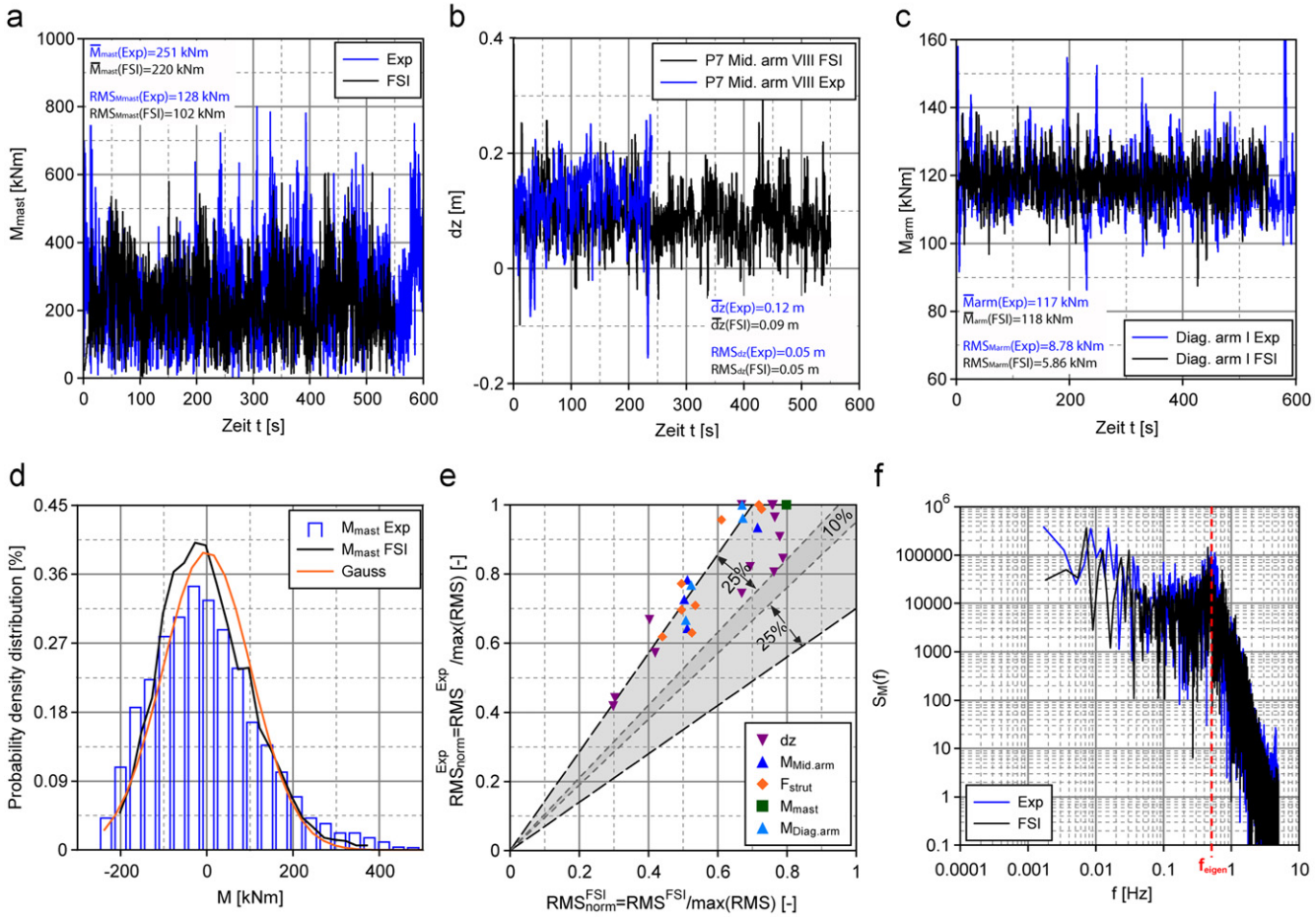

Fig. 11. Results of FSI simulation with a short inflow length in comparison with measurements: (a) mast foot moment; (b) vertical arm tip displacement dz at point P7; (c) cantilever moment diagonal arm VII; (d) probability density distribution mast foot moment; (e) comparison of normalized RMS values of FSI simulation and experiment; and (f) spectral density distribution mast foot moment.

A true comparison, i.e. validation, can only be made in the statistical sense by comparing statistical result data derived from long duration wind load simulations. This is because wind loads generated by the atmospheric turbulent boundary layer are chaotic in nature, and attempts to find repetitive deterministic intervals will fail. It is known that most of the representative micro-meteorological statistical data can be extracted from winds with 10 min duration. Therefore the deterministic FSI simulation was performed for 600 s physical duration.

Within this paper normal forces in the upper strut (F_{strut}), bending moments at the lower support of the middle arms ($M_{Mid.arm}$) and diagonal arms ($M_{Diag.arm}$), arm tip deflection (dz) and mast foot moment (M_{mast}) of the measurement (e.g. M_{mast}(Exp)) are compared with simulation results (e.g. M_{mast}(FSI)) (Fig. 9b and d).

Fig. 9e shows the time history of the mast foot moment over a period of 10 min. It is evident that the results from simulation and experiment differ from each other significantly. Both, the time averaged and the fluctuation values of the mast foot moment were underestimated by about 50% within the simulation (avge M_{Mast}(Exp)=251 kNm, avge M_{Mast}(FSI)=125 kNm). Furthermore, the response spectrum of the mast foot moment in the simulation is not correctly reproduced (Fig. 9f). The first natural frequency of the umbrella is at 0.5–0.6 Hz, which is slightly below the numerically determined first natural frequency. The reason is that compared to the ideal structure model, both the mass of the surrounding volume of air and stiffness differences of the built umbrella are not considered within the eigenmode analysis. The dynamic amplification, visible in the response spectrum at the natural frequency of the umbrella, is not covered within the simulation. Fig. 9g compares the normalized RMS values of the umbrella response. All umbrella reactions (forces, moments and arm tip displacements) from the simulation and experiment were normalized with their maximum and compared with each other. A perfect match would be achieved if all points would lie in the diagram on the 45° angle bisecting line. The dark gray area shows the uncertainty of ±5% resulting from the strain gauge measurements. Most of the evaluated points lie within a limit of +60%. This means that the simulation underestimates the experiment by about 60%. As discussed previously, the high-frequency fluctuation of the wind flow were lost during the long transfer to the reference position of the measuring towers ($f > 0.2$ Hz, Fig. 8c). The result of a CFD simulation with 25 million elements (refinement of the computational grid in upstream direction) shows that the transport of high frequencies is improved only slightly. As an FSI simulation with this high grid resolution on the available hardware with reasonable computation time was not feasible, the numerical calculation area was reduced. The results are shown in the following section.

4.2. Simulation with a short inflow length

4.2.1. CFD simulation

In a second flow simulation, the inflow length was decreased to a minimum value taking into consideration the COST

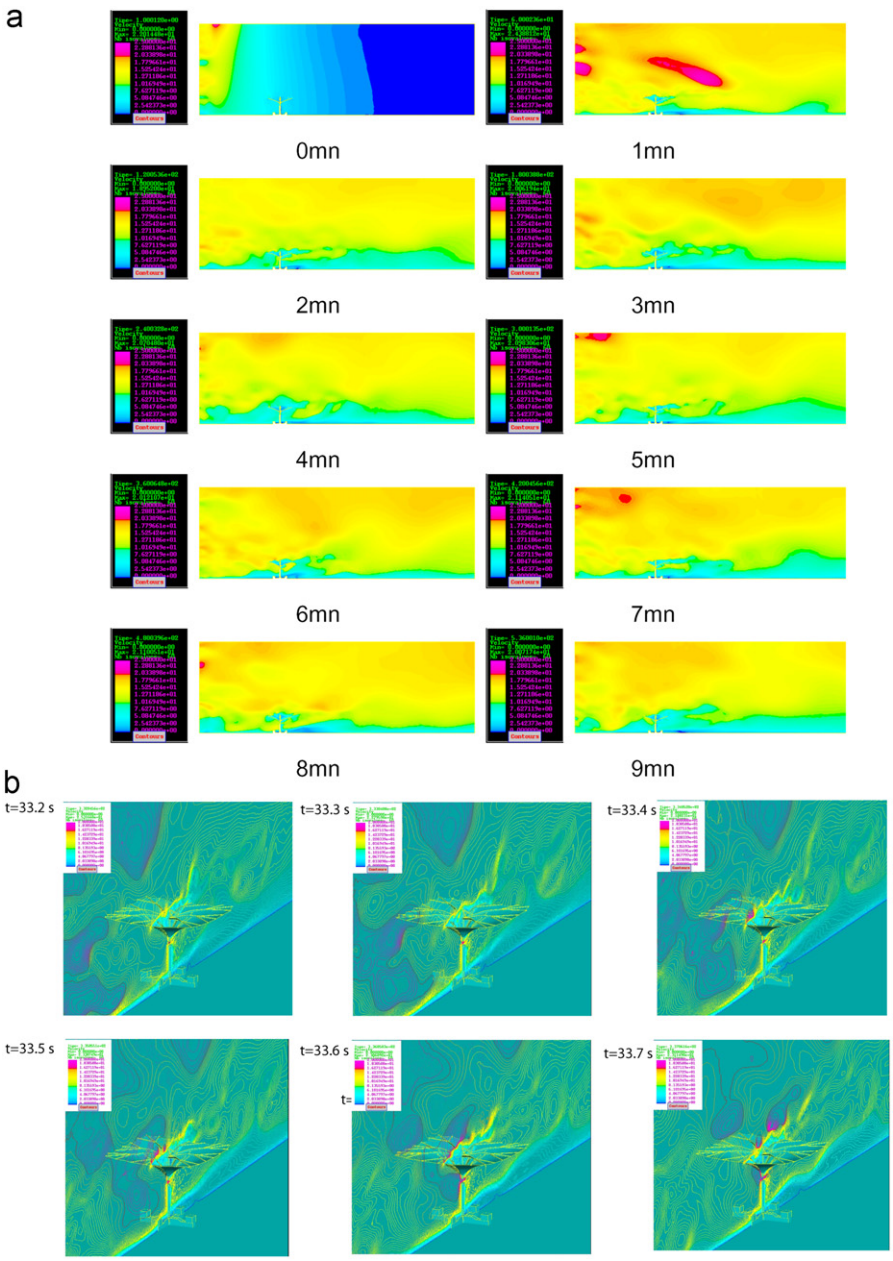

Fig. 12. Fluid–structure interaction simulation: (a) wind velocity contours at vertical x–z cutplane from 0 to 9 min; and (b) isometric views of time snapshots of the wind velocity distribution over the umbrella vertical mid-plane in wind direction in a small time interval from $t=33$–33.8 s).

recommendations (Franke et al., 2004). The constraint of modeling an equilibrium boundary layer in the LES simulation is relaxed within this case. The CFD domain with 14.7 million tetrahedral elements was applied in order to resolve turbulent time scales up to a frequency of 0.6 Hz (Fig. 10e).

The same numerical parameters as prescribed in Section 4.1.1 are used here. The time step is 0.7×10^{-1} s. Fig. 10 shows a good agreement between wind data derived from the in situ measurements and the same data derived from the simulation with the generated synthetic wind field. The evaluation of the gust spectra of the CFD simulation (Fig. 10e) shows a drop in the upper frequency range around 0.5 Hz (vs. 0.2 Hz at long inflow length). Hence, the turbulent scales in the higher frequency range are reproduced better than in the first simulation. The overall agreement of the synthetic wind field is considered as good for most of the statistical quantities (Fig. 10b–f). The generated wind field can now be applied in the FSI simulation of the umbrella.

4.2.2. Fluid–structure interaction simulation

Fig. 11a–c shows that in general there is considerable similarity between the time averaged and the fluctuating values of the experimental and numerical results. The time averaged mast foot moments differ about 14% (vs. 50%), the root-mean-squares about 26% (Fig. 11a). The cantilever moment at the diagonal arm of the FSI simulation (M_{arm}(FSI)$=113$ kNm) matches the experimental results (M_{arm}(Exp)$=117$ kNm) (Fig. 11c). There is also a correspondence of the root-mean-squares. The fluctuating values of the vertical arm tip displacement at the middle arm in windward direction (Arm VIII, see Fig. 5 (right)) agree with the experimental results (Fig. 11b). The time average of the displacement dz within a measurement period of 240 s (due to the limited memory space of the photogrammetric measurement system) is under-predicted in the simulation. More obvious differences between full-scale and FSI simulation were observed at the RMS values shown in Fig. 11e and the peak values. This may be due to the absence of

small-scale turbulence (>0.5 Hz, see Fig. 10e) in the oncoming flow or due to the modeling of flow characteristics around the umbrella. The normalized RMS values of the arm and mast foot moments (M_{arm}, M_{mast}), the vertical arm tip displacements (dz) and the strut force (F_{strut}) resulting from the FSI simulation are within a range of 25% compared to the experimental results. Furthermore, it can be seen that the refinement of the computational grid of flow domain leads to a reduction of the deviation of the RMS values of 60% (Fig. 9e) to 25% (Fig. 11e).

The spectral density distribution of the mast response (Fig. 11f) determined by the numerical simulation, here in terms of the mast foot moment, matches the experimental results. The dynamic amplification is significantly represented at the 1st natural frequency of the system.

The probability density distribution of the numerical computed mast foot moment is approximated with moderate quality by a normal distribution (Fig. 11d). The experimental RMS values are underestimated especially in the region of high fluctuations. Nevertheless, for structural engineering purposes, the instantaneous values of the mast foot moment could be prescribed through a Gaussian distribution with sufficient accuracy. Thus, the statistical analysis was carried out by mean values and standard deviations. Wind velocity contours in a vertical x–z cutplane and isometric views of time snapshots of the umbrella are shown in Fig. 12.

The pressure convergence of the simulation with the small domain (fine grid) was more easily achieved than in the simulation with the long domain (coarse grid) which leads to comparable computational time.

5. Summary

FSI simulations have been performed for the determination of the structural response of a 29 m umbrella under transient wind loads. An innovative synthetic wind velocity field generation technique (Michalski, 2010) permits to model unsteady wind inflow boundary conditions with realistic micro-meteorological statistical properties within a Large Eddy Simulation. The CFD simulation results demonstrated that an in situ measured wind field could be reproduced with its important statistical characteristics.

The simulated structural response of the umbrella is compared with experimentally determined forces and deformations from measurements. A true comparison is made in the statistical sense by comparing statistical result data derived from long duration wind load simulations.

Results of the force and deflection measurements match results from the numerical simulation in a statistical manner within a range of $\pm 25\%$ for the major part of the fluctuating responses (whereas the numerical results are in general smaller than the experimental ones). A comparison of the FSI simulation results of Sections 4.1.2 and 4.2.2 shows that this range could be minimized by refining the numerical CFD model. Computationally intensive investigations, using further refined CFD domains on HPC installations, are now under way, aiming to confirm the observed convergence in accuracy of the results, and in order to determine the required level of model refinement for achieving industrially meaningful results.

As results of the force and deflection measurements match the results of the numerical simulation in a statistical manner, a great step towards the validation and industrial feasibility of the numerical methodology for deformable wind-loaded flexible structures has been accomplished. The evaluation of the results allows the conclusion that the FSI simulation is capable to be applied as an industrial design and engineering tool, especially for lightweight structures showing highly flexible characteristics under transient wind effects. Care must be taken, resolving the turbulence spectrum of the incoming atmospheric boundary layer flow in the CFD simulation depending on the natural frequency of the structural system (here at least up to 0.5 Hz).

References

Journal papers:

Aubry, R., et al., 2008. Deflated preconditioned conjugate gradient solvers for the pressure-Poisson equation. Journal of Computational Physics 227 (24), 10196–10208.

Barnes, M., 1994. Form and stress engineering of tension structures. Structural Engineering Review 6, 175–202.

Bletzinger, K.-U., Ramm, E., 1999. A general finite element approach to the form finding of tensile structures. International Journal of Space Structures 14 (2), 131–145.

Bletzinger, K.-U., et al., 2005. Computational methods for form finding and optimization of shells and membranes. Computational Methods in Applied Mechanics and Engineering 194, 3438–3452.

Bletzinger, K.-U., et al., 2009. Extended and integrated numerical form finding and patterning of membrane structures. Journal of the International Association for Shell and Spatial Structures 50 (1), 35–49.

Bletzinger, K.-U., et al., 2010. Optimal shapes of mechanically motivated surfaces. Computational Methods in Applied Mechanics and Engineering 199, 324–333.

Cebral, J.R., Löhner, R., 1997a. Conservative load projection and tracking for fluid–structure problems. AIAA Journal 35 (4), 687–692.

Cebral, J.R. and Löhner, R. 1997b. Fluid–Structure Coupling: Extensions and Improvements; AIAA-97-0858 (1997).

Deodatis, G., Shinozuka, M., 1991. Simulation of stochastic processes by spectral representation. Applied Mechanics Review 44, 191–203.

Glück, M., 2003. Ein Beitrag zur numerischen Simulation von Fluid-Struktur-Interaktionen - Grundlagenuntersuchung und Anwendung auf Membrantragwerke. Ph.D. thesis, University Erlangen-Nürnberg.

Haug, E, et al., 2009. Industrial design and analysis of structural membranes. International Journal of Space Structures 24 (4).

Haug, E. et al. 1991. The numerical simulation of the inflation process of space rigidized antenna structures. In: Proceedings of the International Conference on Spacecraft Structures and Mechanical Testing, Noordwijk, Netherlands.

Haug, E., Scharnhorst, T., Du Bois, P., 1986. FEM-Crash, Berechnung eines Fahrzeugfrontalaufpralls. VDI Berichte 613, 479–505.

Haug, E. de Rouvray, A., 1984. Finite element design of a high pressure balloon with PAM-LISA. In: AIAA 8th Aerodynamic Decelerator and Balloon Technology Conference, 2–4 April, Jyannis, Massachussetts.

Haug, E., 1981. Engineering safety analysis via destructive numerical experiments, EUROMECH 121, Polish Academy of Sciences. Engineering Transactions 29 (1), 39–49.

Haug, E., 1972. Finite element analysis of pneumatic structures. In: IASS Symposium of Pneumatic Structures, Delft.

Kaiser, U. 2004. Windeinwirkung auf schwach vorgespannte Membranstrukturen am Beispiel eines 30 m Membranschirmes. Ph.D. thesis, Institut of Aerodynamic and Gasdynamics of the University of Stuttgart.

Kawamura, S., Kiuchi, T., 1986. An experimental study of one-membrane type pneumatic structure — wind load response. Journal of Wind Engineering and Industrial Aerodynamics 23, 127–140.

Kind, R.J., 1984. Pneumatic stiffness and damping of air-supported structures. Journal of Wind Engineering and Industrial Aerodynamics 17, 295–304.

Kimoto, E., Kawamura, S, 1983. Aerodynamic behaviour of one-way type hanging roofs. Journal of Wind Engineering and Industrial Aerodynamics 13, 395–405.

Kunieda, H., 1975. Flutter of hanging roofs and curved membrane roofs. International Journal of Solids Structures, 477–492.

Löhner, R., et al., 2006. Improving the speed and accuracy of projection-type incompressible flow solvers. Computer Methods in Applied Mechanics and Engineering 195 (23–24), 3087–3109.

Löhner, R., 2005. Projective prediction of pressure increments. Communications in Numerical Methods in Engineering 21 (4), 201–207.

Löhner, R., 2004. Multistage explicit advective prediction for projection-type incompressible flow solvers. Journal of Computational Physics 195, 143–152.

Löhner, R., 1998. Renumbering strategies for unstructured-grid solvers operating on shared-memory, Cache-Based Parallel Machines. Computer Methods in Applied Mechanics and Engineering 163, 95–109.

Löhner, R. et al., 1995. Fluid–structure interaction using a loose coupling algorithm and adaptive unstructured grids; AIAA-95-2259 [Invited].

Löhner, R. et al., 1994. New Advances in fluid structure interaction, Basel world CFD user days 1994. In: Conference Proceedings 24.1-24.20.

Löhner, R., 1993. Some useful renumbering strategies for unstructured grids. International Journal of Numerical Methods in Engineering 36, 3259–3270.

Mann, J., 1998. Wind field simulation. Probabilistic Engineering Mechanics 13 (4), 269–282.

Michalski, A., et al., 2009. Virtual design methodology for lightweight structures – aerodynamic response of membrane structures. International Journal of Space Structures 24 (4), 211–221.

Newman, B.G., Ganguli, U., 1984. Flow over spherical inflated buildings. Journal of Wind Engineering and Industrial Aerodynamics 17, 305–327.
Rossi, R., et al., 2004. Wind field simulation for structural engineering purposes. International Journal for Numerical Methods in Engineering 61, 738–763.
Schek, H.-J., 1974. The force density method for form finding and computations of general networks. Computer Methods in Applied Mechanics and Engineering 3, 115–134.
Shinozuka, M., Jan, C.-M., 1972. Digital simulation of random processes and its applications. Journal of Sound and Vibration 25, 111–128.
Wüchner, R., Bletzinger, K.-U., 2005. Stress-adapted numerical form finding of prestressed surfaces by the updated reference strategy. International Journal for Numerical Methods in Engineering 64, 143–166.
Wüchner, R., et al., 2007. A framework for stabilized partitioned analysis of thin membrane–wind interaction. International Journal for Numerical Methods in Fluids 54, 945–963.

Monographs, Multi-author volumes, Proceedings:

Franke, J. et al. 2004. Recommendations on the use of CFD in predicting pedestrian wind environment COST Action C14.
Haug E., 1988. Numerical Form-Finding of Membranes. IL 18 Seifenblasen. Institut für Leichte Flächentragwerke Universität Stuttgart, 1988.
Haug, E., Powell, G.H., 1972. Finite element analysis of nonlinear membrane structures. Report no. SESM72-7, Structural Engineering Laboratory, University of California, Berkeley, California, February 1972.
Löhner, R., 2008. Applied Computational Fluid Dynamics Techniques. 2nd edition, John Wiley.
Mann, J., 1994. Models in micrometeorology. Technical report, Risoe National Laboratory, Roskilde, Denmark, 1994.
Michalski, A., 2010. Numerische Simulation leichter Flächentragwerke in einer numerisch generierten atmosphärischen Grenzschicht, Ph.D. thesis at the Chair of Structural Analysis, Technical University Munich.
Michalski, A., et al., 2007. On the application of the fluid structure interaction simulation for the design of umbrella structures. In: International Conference on Textile Composites and Inflatable Structures Barcelona.
Rosemeier, G., 2008. Windbelastung von Bauwerken. Bauwerk Verlag GmbH.
Vetterling, W.T., et al., 2001. Numerical Recipes in Fortran 77, The Art of Scientific Computing, 2nd edition Campridge University Press.
Wüchner, R., 2006. Mechanik und Numerik der Formfindung und Fluid-Struktur-Interaktion von Membrantragwerken, Ph.D. thesis, Chair of Structural Analysis, Technical University Munich.